An Iron(II) Complex Exhibiting Five Anhydrous Phases, Two of Which Interconvert by Spin-Crossover with Wide Hysteresis

Thomas D. Roberts,[a] Floriana Tuna,[b] Tamsin L. Malkin,[c] Colin A. Kilner,[a] and Malcolm A. Halcrow[a]*

[a]School of Chemistry, University of Leeds, Woodhouse Lane, Leeds, UK LS2 9JT.
E-mail: m.a.halcrow@leeds.ac.uk
[b]School of Chemistry, University of Manchester, Oxford Road, Manchester, UK M13 9PL.
[c]Institute for Climate & Atmospheric Science, School of Earth and Environment, University of Leeds, Leeds, UK LS2 9JT.

Supporting Information

Experimental Details

Scheme S1. Synthesis of 2,6-*bis*[5-methylpyrazol-3-yl]pyridine (*L*).

Table S1. Experimental data for the single crystal structure determinations in this work.

Figure S1. View of the asymmetric unit in $L \cdot CH_3OH$.

Figure S2. Partial packing diagram of $L \cdot CH_3OH$.

Figure S3. View of the complex molecule in the structure of $\mathbf{1^A}$ at 300 K.

Figure S4. Diagram of $\mathbf{1^A}$, showing disorder of the BF_4^- ion between two different hydrogen bonding sites.

Table S2. Hydrogen bond parameters in the crystal structures in this work.

Figure S5. Thermogravimetric analyses of $\mathbf{1} \cdot 2H_2O$.

Figure S6. Observed or simulated *X*-ray powder diffraction patterns of the different phases of **1**.

Figure S7. Comparison of the measured *X*-ray powder patterns of the different phases of **1**, during the first and the fifth consecutive thermal cycles *in vacuo*.

Experimental

Ligand L was synthesised by an alternative to the published method (Scheme S1).[1] All other reagents and solvents were used as commercially supplied, without further purification.

Synthesis of 2,6-*bis*[3-dimethylaminobut-2-en-1-onyl]pyridine A solution of 2,6-diacetylpyridine (10.0 g, 61.3 mol) in dimethylformamide dimethylacetamide (50 g, 376 mmol) was refluxed for 16 hrs under N_2. The resultant brown precipitate was collected by filtration, washed with acetone and dried *in vacuo*. Yield 12.0 g, 65 %. Found: C, 67.5; H, 7.65; N, 13.9 %. Calcd for $C_{17}H_{23}N_3O_2$ C, 67.7; H, 7.69; N, 13.9 %. M.p. 234-235 °C. ES mass spectrum: m/z 302.2 $[MH]^+$. ^1H NMR ($CDCl_3$): δ 2.65 (6H, s, CH_3C), 3.05 (12H, s, N$\{CH_3\}_2$), 6.75 (2H, s, C=CH–CO), 7.81 (1H, t, 7.8 Hz, Py H^4), 8.14 (2H, d, 7.8 Hz, Py $H^{3/5}$). ^{13}C NMR ($CDCl_3$): δ 16.9 (CH_3C), 40.4 (4C, N$\{CH_3\}_2$), 91.3 (2C, C=CH–CO), 123.4 (2C, Py $C^{3/5}$), 137.8 (1C, Py C^4), 156.3 (2C, Py $C^{2/6}$), 165.1 (2C, Me$C\{NMe_2\}$=C), 185.9 (2C, CO).

Synthesis of 2,6-*bis*[5-methyl-1*H*-pyrazol-3-yl]pyridine methanol solvate ($L\cdot CH_3OH$) A mixture of 2,6-*bis*-[3-dimethylaminobut-2-en-1-onyl]pyridine (6.0 g, 19.9 mol) and hydrazine hydrate (6.0 g, 118 mmol) in methanol (75 cm^3) was refluxed for 16 hrs. The resultant pale yellow solution was concentrated until an off-white precipitate appeared. This was collected, washed with water, and dried *in vacuo*. Yield 3.9 g, 82 %. Found: C, 62.9; H, 6.60; N, 25.8 %. Calcd for $C_{13}H_{13}N_5\cdot CH_3OH$ C, 62.0; H, 6.32; N, 25.3 %. M.p. 215-216 °C. ES mass spectrum: m/z 240.1 $[LH]^+$. ^1H NMR ($CDCl_3$): δ 2.29 (6H, s, CH_3), 6.74 (2H, s, Pz H^4), 7.73 (2H, d, 7.6 Hz, Py $H^{3/5}$), 8.84 (1H, 7, 7.6 Hz, Py H^4), 12.70 and 13.04 (combined integral 2H, both br s, NH). ^{13}C NMR ($\{CD_3\}_2SO$): δ 13.0 (2C, CH_3), 104.1 (2C, Pz C^4), 119.2 (2C, Py $C^{3/5}$), 138.9 (1C, Py C^4). The presence of methanol in the material was confirmed by a crystal structure determination, described below.

Synthesis of $[FeL_2][BF_4]_2\cdot 2H_2O$ ($1\cdot 2H_2O$) A solution of $L\cdot CH_3OH$ (0.28 g, 1.05 mmol) and $Fe[BF_4]_2\cdot 6H_2O$ (0.18 g, 0.52 mmol) in MeOH (25 cm^3) was stirred until all the solid had dissolved. The resultant solution was filtered, and concentrated to *ca.* 5 cm^3. Slow diffusion of diethyl ether vapour into this solution yielded large brown blocks, that were isolated by filtration and washed with diethyl ether, air dried and analysed without further purification. Yield 0.26 g, 68 %. Freshly prepared sample. Found: C, 42.2; H, 3.95; N, 18.9 %. Calcd for $C_{26}H_{26}B_2F_8FeN_{10}\cdot 2H_2O$ C, 42.0; H, 4.06; N, 18.8 %. Following dehydration/rehydration. Found: C, 42.6; H, 3.95; N, 17.4 %. Calcd for $C_{26}H_{26}B_2F_8FeN_{10}\cdot 2H_2O$ C, 42.0; H, 4.06; N, 18.8 %. ES mass spectrum: m/z 240.1 $[LH]^+$, 267.1 $[FeL_2]^{2+}$, 533.2 $[FeL_2–H]^+$, 621.2 $[FeL_2BF_4]^+$. IR spectrum (nujol): 3608s, 3535m, 3326s, 3157w, 3133w, 3053w, 2731w, 1615m, 1578s, 1519m, 1305w, 1285s, 1262w, 1235m, 1189m, 1158w, 1123m, 1060vs, 978w, 882br m, 830w, 809s, 795s, 754w, 746w, 699w, 681w, 663w, 638w, 520w cm^{-1}.
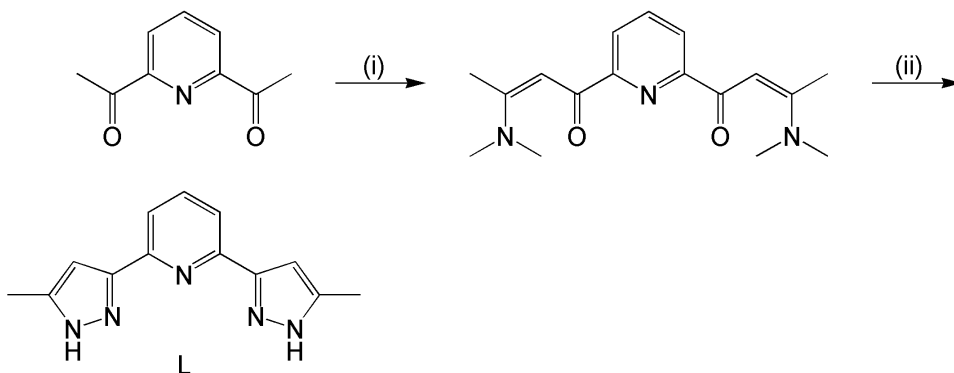
Scheme S1. Synthesis of 2,6-*bis*[5-methylpyrazol-3-yl]pyridine (L). Reagents and conditions: (i) dimethylacetamide dimethylacetal, reflux, 16 hrs. (ii) hydrazine hydrate, ethanol, reflux.

Single crystal *X*-ray structure determinations

Slow diffusion of diethyl ether vapour into a methanolic solution of *L* afforded colourless prisms of *L*·CH$_3$OH. Brown blocks of **1**·2H$_2$O were similarly grown by diffusion of diethyl ether vapour into a nitromethane solution of the complex, while yellow prisms of **1**^{A} were sometimes obtained by vapour diffusion of diethyl ether into a solution of the compound in dry methanol. Experimental details of these structure determinations are given in Table S1. All diffraction data were measured using a Bruker X8 Apex II diffractometer, with graphite-monochromated Mo-K_α radiation (λ = 0.71073 Å) generated by a rotating anode. The diffractometer was fitted with an Oxford Cryostream nitrogen low temperature device. The structures were solved by direct methods using SHELXS97,[2] and developed by full least-squares refinement on F^2 (SHELXL97[2]). Crystallographic figures were prepared using XSEED,[3] which incorporates POVRAY.[4]

No disorder was detected during the refinement of *L*·CH$_3$OH, and no restraints were applied. All non-H atoms were refined anisotropically. Since not all H atoms could be located in the Fourier map, all C-bound H atoms were placed in calculated positions and refined using a riding model. The N- and O-bound H atoms were all located, and were allowed to refine freely with a common U_{iso} displacement parameter. Since there are no heavy atoms in the crystal its absolute structure could not be determined. Therefore, the Friedel opposites in the data were merged for the final cycles of least-squares refinement. CCDC 836792.

The asymmetric unit of **1**·2H$_2$O contains two unique quarter-cations. The cation centred on Fe(1) lies on the S_4 site 0, ¼, $^1/_8$, with N(2) and C(5) on the C_2 axis [0, ¼, *z*], while the other cation [Fe(12)] occupies the S_4 site ½, ¾, $^1/_8$, with N(13) and C(16) spanning the C_2 axis [½, ¾, *z*]. The model also contains one BF$_4^-$ ion and one water molecule lying on general crystallogaphic positions. No disorder was detected during refinement, and no restraints were applied. All non-H atoms were refined anisotropically, and C- and N-bound H atoms were placed in calculated positions and refined using a riding model. The water H atoms were located in the difference map, and allowed to refine freely. The two O–H distances both refined to 0.84(3) Å. CCDC 836761

Following a cycle of dehydration at 375 K and rehydration at 300 K, the same crystal afforded an identical unit cell within experimental error at 150 K: tetragonal *I*, *a* = 13.751(3), *c* = 35.387(7) Å, *V* = 6691(2) Å^3. An attempted refinement of these data starting from the original structure solution was unsusccessful, however. Examination of the diffraction images showed some peak splitting but no double diffraction pattern, showing that the crystal had become twinned during the dehydration/rehydration process.

Different crystals were used for the two structures of **1**^{A}, because the original crystal had degraded significantly upon rewarming from 150 K to room temperature. The asymmetric unit of **1**^{A} also contains ¼ of a complex dication, with Fe(1) occupying the crystallographic S_4 site [¼, ¼, ¼] and N(2) and C(5) lying on the C_2 axis [¼, ¼, *z*]; and, half a BF$_4^-$ anion that is disordered about the C_2 axis [¼, ¾, *z*]. Two equally occupied partial environments for this disordered half-anion were refined at 150 K, which shared a common half-occupied B atom B(12). These were subject to the refined restraints B–F = 1.42(2) and F...F = 2.32(2) Å. At 300 K, three disorder sites for the anion were refined with occupancies 0.25, 0.20 and 0.05, again sharing a common half-occupied B atom. The restraints at this temperature refined to the different values of B–F = 1.38(2) and F...F = 2.25(2) Å. At both temperatures, all non-H atoms except the disordered F atoms were refined anisotropically, and all H atoms were placed in calculated positions and refined using a riding model. The refinement at 300 K was performed with unit weights, leading to a high goodness-of-fit. CCDC 836762 and 836763.

Table S1 Experimental data for the single crystal structure determinations in this work.

|	$L \cdot CH_3OH$	$1 \cdot 2H_2O$	1^A, high-spin[c]	1^A, low-spin[c]
Molecular formula	$C_{14}H_{17}N_5O$	$C_{26}H_{30}B_2F_8FeN_{10}O_2$	$C_{26}H_{26}B_2F_8FeN_{10}$	$C_{26}H_{26}B_2F_8FeN_{10}$
M_r	271.33	744.07	708.04	708.04
Crystal class	Orthorhombic	Tetragonal	Tetragonal	Tetragonal
Space group	$P2_12_12_1$	$I4_1/a$	$P4_2/n$	$P4_2/n$
a (Å)	10.0640(4)	13.7494(19)	9.8046(5)	9.7481(2)
b (Å)	11.6546(5)	–	–	–
c (Å)	12.3944(6)	35.336(3)	17.8869(13)	17.6848(5)
V (Å^3)	1453.76(11)	6680.2(14)	1719.47(18)	1680.51(7)
Z	4	8	2	2
μ (Mo-K_α) (mm^{-1})	0.083	0.538	0.515	0.527
T (K)	150(2)	150(2)	300(2)	150(2)
Measured reflections	25693	35446	29025	29002
Independent reflections	204	4363	2165	2179
R_{int}	0.076	0.086	0.070	0.054
$R(F)$[a]	0.065	0.043	0.080	0.091
$wR(F^2)$[b]	0.184	0.121	0.272	0.288
Goodness of fit	1.099	1.009	2.110	1.099

[a]$R = \Sigma[|F_o| - |F_c|] / \Sigma|F_o|$ [b]$wR = [\Sigma w(F_o^2 - F_c^2) / \Sigma w F_o^4]^{1/2}$
[c]Different crystals were used for these two structure determinations.

Other measurements

Elemental microanalyses were performed by the University of Leeds School of Chemistry microanalytical service. ^1H and ^{13}C NMR spectra employed a Bruker DPX300 spectrometer operating at 300.2 MHz. Electrospray mass spectra were obtained using a Waters Micromass LCT TOF spectrometer, from MeCN solution. The TGA measurement employed a TA Instruments TGA 2050 analyser. Magnetic susceptibility measurements were performed on a Quantum Design SQUID magnetometer, in an applied field of 5000 G. A temperature ramp of 2 K min^{-1} was used for these measurements, unless otherwise stated. A diamagnetic correction for the sample was estimated from Pascal's constants;[5] a diamagnetic correction for the sample holder was also applied. *X*-ray powder diffraction measurements were obtained with a Bruker D8 Advance A25 diffractometer, using Cu-K_α radiation (λ = 1.5418 Å) radiation. The samples were measured in an ambient atmosphere as a layer of powder, but were ground into a nujol mull for measurements under vacuum. That is the origin of the reduced signal-to-noise ratio in the *in vacuo* measurements (Figs. 6, S6 and S7).

[1]   Y. Zhou, W. Chen and D. Wang, *Dalton Trans.*, 2008, 1444.
[2]   G. M. Sheldrick, *Acta Crystallogr., Sect. A*, 2008, **64**, 112
[3]   L. J. Barbour, *J. Supramol. Chem.*, 2001, **1**, 189.
[4]   *POVRAY v. 3.5*, Persistence of Vision Raytracer Pty. Ltd., Williamstown, Victoria, Australia, 2002. http://www.povray.org.
[5]   C. J. O'Connor, *Prog. Inorg. Chem.*, 1982, **29**, 203.
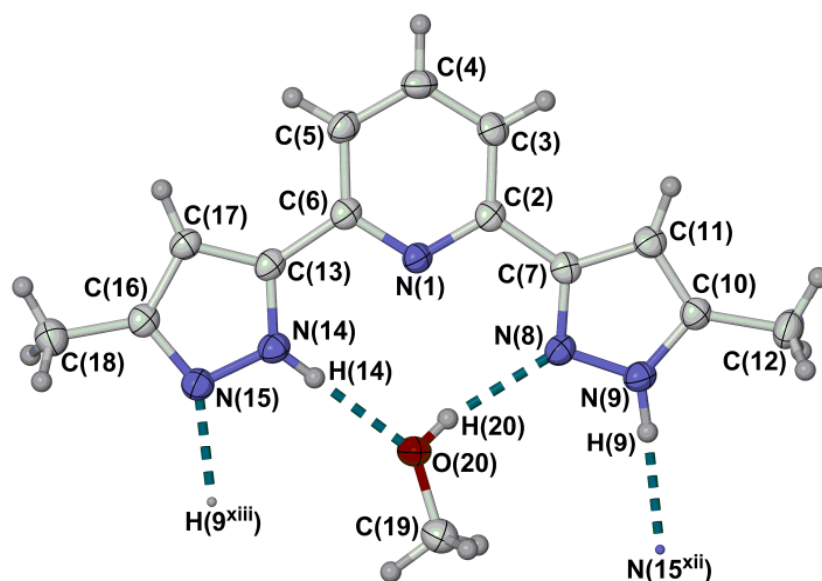
Fig. S1 View of the asymmetric unit in $L \cdot CH_3OH$, showing the atom numbering scheme employed. Thermal ellipsoids are at the 50% probability level, except for H atoms which have arbitrary radii. Symmetry codes: (xii) $-\frac{1}{2}+x$, $\frac{1}{2}-y$, $1-z$; (xiii) $\frac{1}{2}+x$, $\frac{1}{2}-y$, $1-z$. Colour code: C, white; H, grey; N, blue; O, red.
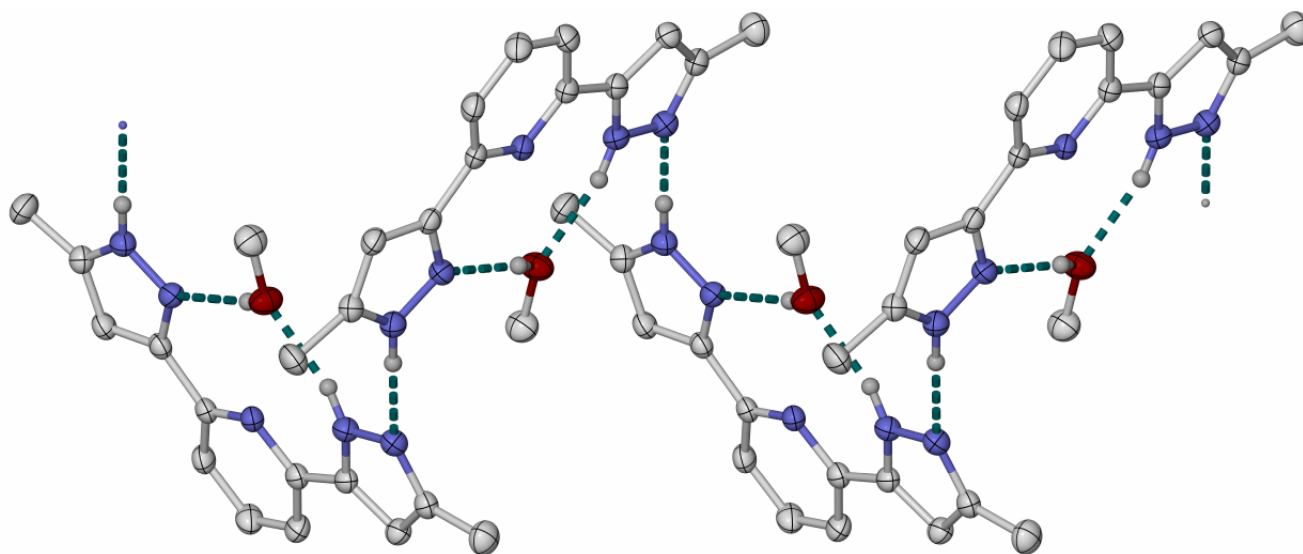

Fig. S2 Partial packing diagram of $L \cdot CH_3OH$, showing the association of the molecule into hydrogen bonded chains zig-zagging along the unit cell *a* axis. The view is perpendicular to the crystallographic (010) plane.. Thermal ellipsoids are at the 50% probability level, except for H atoms which have arbitrary radii, and all C-bound H atoms have been omitted for clarity.
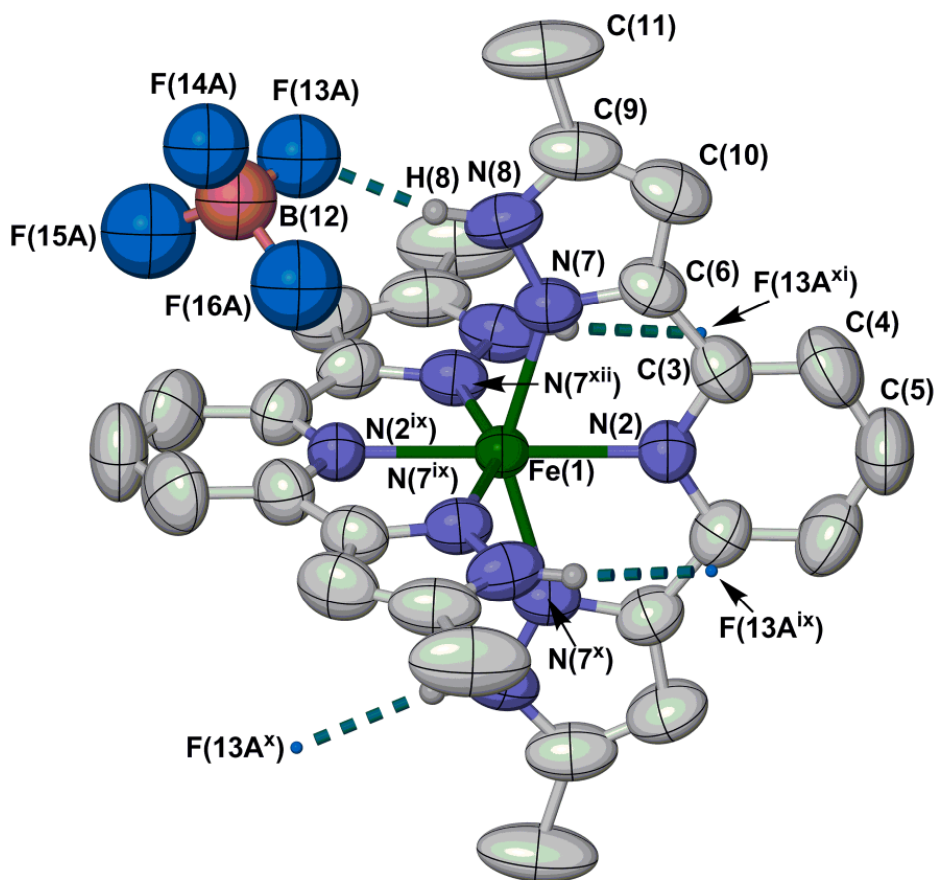
Fig. S3 View of the complex molecule in **1^A** at 300 K, showing the atom numbering scheme employed. Thermal ellipsoids are at the 50% probability level. Only one of the three disorder sites for the unique half-anion is shown, and all C-bound H atoms have been omitted for clarity. Symmetry codes: (ix) y, ½–x, ½–z; (x) ½–x, ½–y, z; (xi) ½–y, x, ½–z. Colour code: C, white; H, grey; B, pink; F, cyan; Fe, green; N, blue.

The anion is disordered about a crystallographic C_2 axis, so that on average only two of the four potential N–H...F hydrogen bonding sites are occupied for each cation (see Fig. S4).
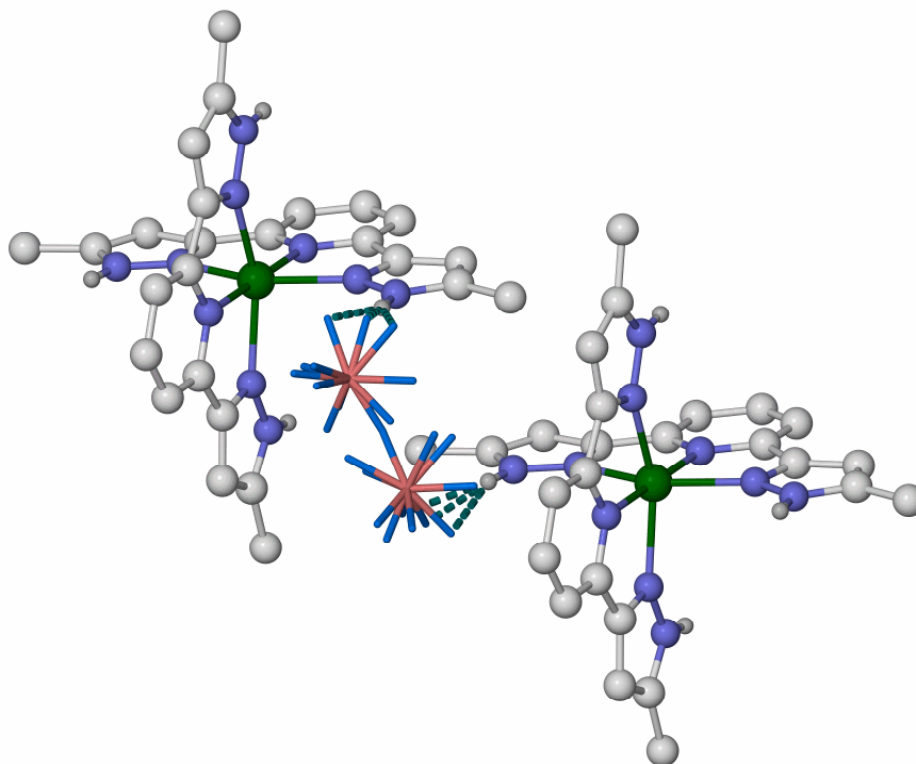
Fig. S4 Diagram of **1^A** at 150 K, showing disorder of the BF$_4^-$ ion between two different hydrogen bonding sites. All three anion disorder sites are shown, in both of their orientations across the C_2 axis. C-bound H atoms have been omitted for clarity, and all atoms have arbitrary radii. Color code: C, white; H, grey; B, pink; F, cyan; Fe, green; N, blue.

Table S2 Hydrogen bond parameters in the crystal structures in this work (Å, °). See Figs. S1, S3 and Fig. 1 of the main paper for the atom numbering schemes employed. Symmetry codes: (vii) ½+x, y, ½–z; (xii) –½+x, ½–y, 1–z.

|	D–H	H...X	D...X	N–H...X
L·CH$_3$OH				
N(9)–H(9)…N(15^{xii})	0.90(4)	1.92(4)	2.817(4)	178(4)
N(14)–H(14)…O(20)	0.85(4)	1.99(4)	2.820(4)	164(4)
O(20)–O(20)…N(8)	0.77(4)	2.12(5)	2.860(4)	163(4)
1·2H$_2$O				
N(8)–H(8)…F(27)	0.88	1.99	2.836(2)	159.7
N(19)–H(19)…O(28)	0.88	1.88	2.744(2)	168.5
O(28)–H(28A)…F(24)	0.84(3)	1.97(3)	2.786(2)	163(3)
O(28)–H(28B)…F(25^{vii})	0.84(3)	1.99(3)	2.797(2)	162(3)
1^A, 300 K				
N(8)–H(8)…F(13A)/F(13B)/F(13C)	0.88	1.88/2.10/2.06	2.735(14)/2.950(10)/2.86(3)	163.8/162.2/152.1
1^A, 150 K				
N(8)–H(8)…F(13A)/F(13B)	0.88	1.98/1.86	2.840(16)/2.71(2)	164.8/164.3
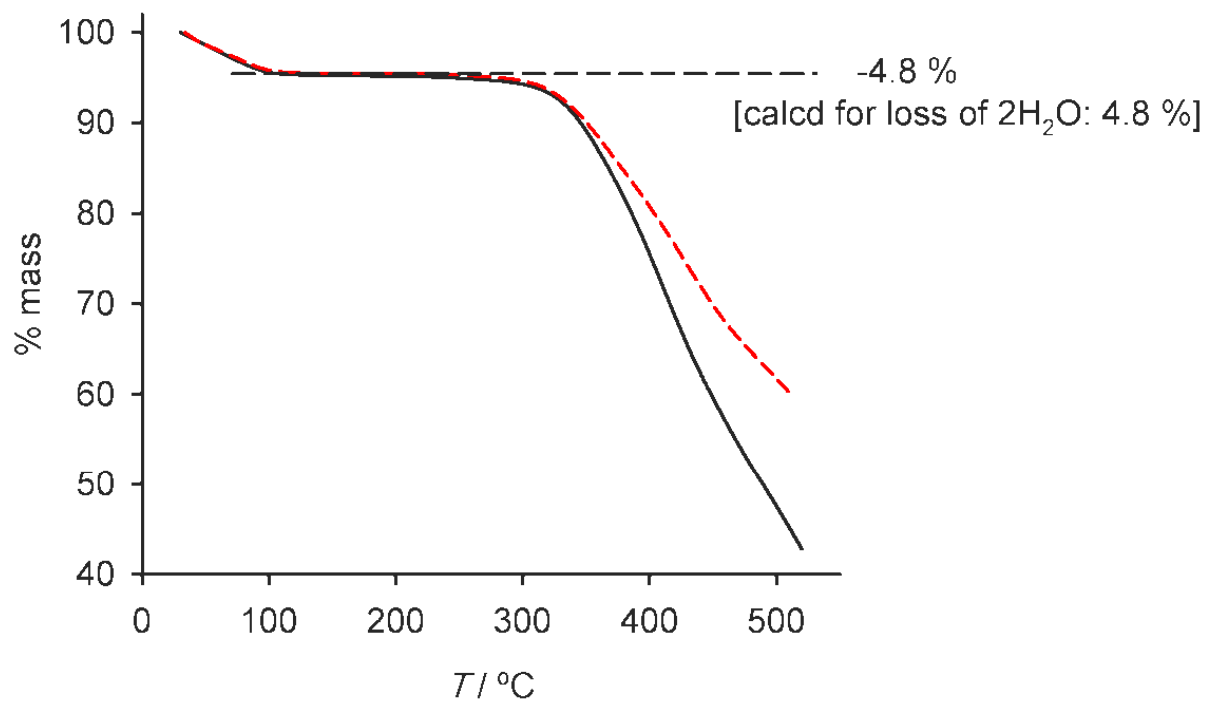
Fig. S5 Thermogravimetric analyses (TGAs) of **1**·2H$_2$O. Analyses of the as-prepared material (black solid line), and a sample that has been dehydrated at 400 K then rehydrated under ambient conditions (red dashed line), are shown.
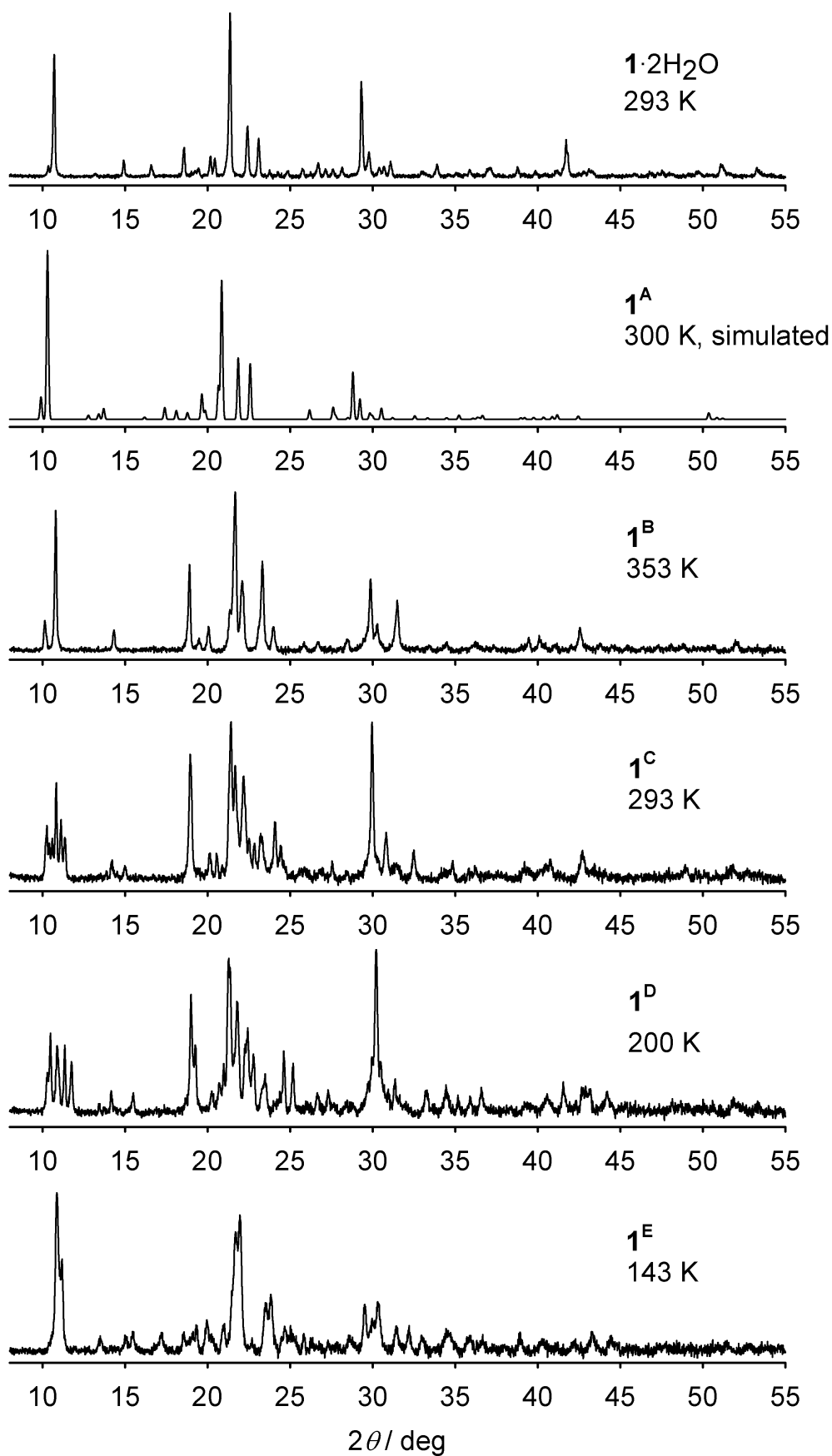
Fig. S6. Observed or simulated *X*-ray powder diffraction patterns of the different phases of **1**. Data for **1**^B^-**1**^E^ are from the first thermal cycle of the sample under vacuum.
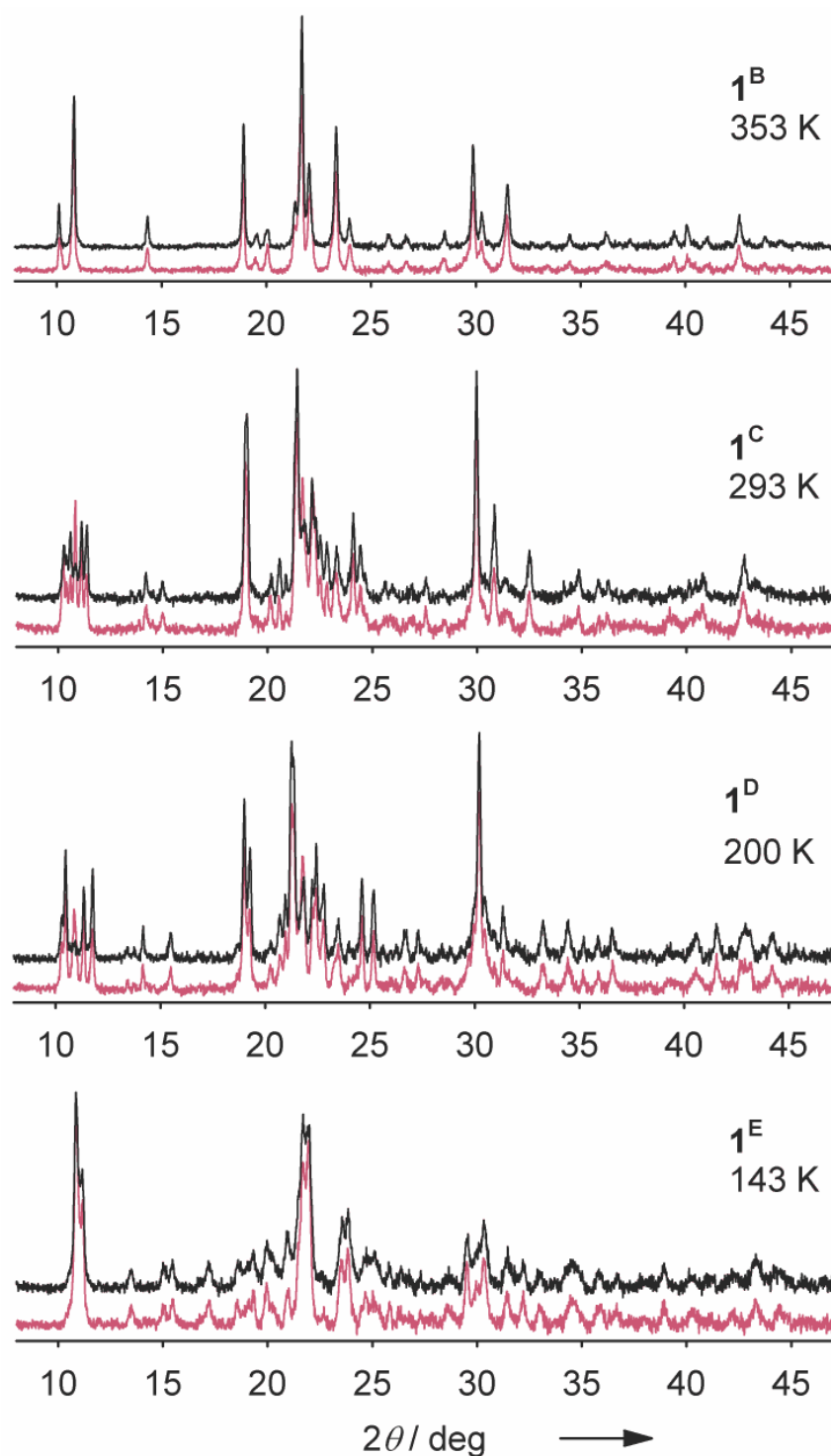
Fig. S7 Comparison of the measured *X*-ray powder patterns of the different phases of **1**, during the first (maroon) and the fifth (black) consecutive thermal cycles *in vacuo*.

There is perfect peak matching in the powder patterns of **1**^{B}-**1**^{E} between the fresh and aged samples. However, for **1**^{C} and **1**^{D} there are differences in the low-angle peak intensities between the two sets of diffractograms. This implies there is a change in the crystallinity of these phases as the sample is aged. That is reasonable, since repeated cycling across the phase transitions should introduce more defects and fractures into the material, making it a more ideal powder.